Paper ID APEN-MIT-2019_66
Applied Energy Symposium: MIT A+B
May 22-24, 2019 • Boston, USA

Design and Optimization of CO_2-WAG Projects Using an Artificial-Intelligence Assisted Computational Framework

Junyu You
Petroleum Recovery Research Center
New Mexico Institute of Mining and Technology
Socorro, NM
junyu.you@student.nmt.edu

William Ampomah
Petroleum Recovery Research Center
New Mexico Institute of Mining and Technology
Socorro, NM
William.Ampomah@nmt.edu

Qian Sun
Petroleum Recovery Research Center
New Mexico Institute of Mining and Technology
Socorro, NM
qian.sun@nmt.edu

Robert Scott Balch
Petroleum Recovery Research Center
New Mexico Institute of Mining and Technology
Socorro, NM
robert.balch@nmt.edu

Martha Cather
Petroleum Recovery Research Center
New Mexico Institute of Mining and Technology
Socorro, NM
martha.cather@nmt.edu

Abstract— In this article, a robust machine-learning based computational framework that couples multi-layer neural network (MLNN) proxies and multi-objective particle swarm optimizer (MOPSO) to design water-alternative-CO_2 injection (CO_2-WAG) projects is presented. The proposed optimization protocol considers various objective functions including oil recovery and CO_2 storage volume. Expert MLNN systems are trained and employed as surrogate models of the high-fidelity compositional simulator in the optimization workflow. A large volume of blind testing applications is employed to confirm the validities of the proxies. When multiple objective functions are considered, two approaches are employed to treat the objectives: the weighted sum method and Pareto-front-based scheme. A field scale implementation to Morrow-B formation at Farnsworth Unit (FWU) to optimize the tertiary recovery strategy is discussed. In this work, investigations will focus on comparing the optimum solution found by the aggregative objective function and the solution repository covered by the Pareto front, which considers the physical and operational constraints and reduces uncertainties involved by the multi-objective optimization process. Necessary trade-offs need to be decided using the solution repository to balance the project economics and **CO_2** storage amount.

Keywords—optimization, carbon dioxide, sequestration, proxy models, multi-objective

I. Introduction

Greenhouse gas (GHG) emission related with human activity has been known as one of primary reasons resulted in global warming issue and gained a lot attention in recent years[1-3]. At the same time, CO_2 flooding is proofed to be an efficient technique to produce more residual oil after a mature field after primary and secondary oil recovery and has been widely used in USA as one Enhanced Oil Recovery (EOR) technique[4-10]. A CO_2 –EOR project would have dual benefits of injecting CO_2 to underground oil reservoirs to improve oil recovery and safely storing a large volume of these injected oil within the rock. This project is also known as a CCUS project, which referring carbon capture, utilization and storage.

The Southwest Regional Partnership on Carbon Sequestration (SWP) is one of seven regional partnerships funded by the US Department of Energy (DOE) to study techniques and strategies on safely and permanently storing of CO_2 in partially depleted oil and gas reservoirs. SWP project is in its Phase III study now, which focuses on an actual CO_2 –EOR field project in Farnsworth Unit (FWU). A rigorous numerical model was established and validated by history matching with the field history. Such numerical model can also be utilized to forecast the oil recovery and track the long-term fate of injected CO_2[7, 8, 11-13]. On the field side, a total amount of 16.82 Bscf of anthropogenic CO_2 was injected into the Morrow B formation in FWU during the time period from December 2010 to December 2014[8]. Promising responses obtained from field implementations indicate that the undergoing CO_2 EOR project is competent to both effectively produce residual oil and safely store CO_2.

As a CCUS project, an ideal development strategy for FWU would seek to maximize both hydrocarbon production and CO_2 sequestration simultaneously, which introduces two objectives to be optimized. Notably, the improvement of oil production may not lead to increments of CO_2 storage, since CO_2 storage needs investment for CO_2 injection. Thus, the maximization of oil production and CO_2 storage can be treated as two conflict objectives. Multi-objective Particle Swarm Optimization (MOPSO) is employed to establish the to find the Pareto front to store the alternative solutions since it is easier to implement and converges faster than other optimization algorithms [14]. MLNN models are trained and coupled with MOPSO to accelerate the optimization protocol. The innovative aspects of this work involve:

(1) Compared with previous optimization work within FWU [7, 8], Pareto optimum is used for the first time to co-optimize oil production and CO_2 sequestration, which are two objectives with conflict relation. Pareto front provides FWU operators more options of the design parameters based on various demands of project outcome.

(2) A hybrid workflow incorporating MOPSO and MLNN is established and demonstrated to be fast, robust and stable. MLNN proxy modeling is capable to mimic nonlinear mapping from operational variables to time-series predictions (e.g. cumulative oil production and CO_2 sequestration). The ability to investigate those two dynamic and time-dependent outputs is important to SWP project, since investigation of how those parameters involves with time will provide SWP scientists more information on geological and porous media fluid properties.

(3) After generating a Pareto front of multiple objectives, a further step is made: a trade-off factor is defined in this work to assist decision maker for make a decision on quick selection of objective values.

(4) Last but not the least, this work will also investigate the difference between the unique optimal solution found using weighted sum method (a classfical method that is wildely used to solve multi-objective optimizaon problem) and Pareto optimal solutions. The comparison between these two methods would show Pareto optimum is able to address the existence of non-unique solution of MOP optimization and show how it influence making a decision.

With the help of developed optimization protocol, engineers of a CCUS project would have more flexibility on project designing such that less trade-off needs to pay when optimizing multiple conflict objectives.

II. METHODOLOGY

In this work, the training data and test data are extracted from a companion work where a total of 597 high-fidelity simulation experiments were conducted as raw data. These 597 numerical simulations are performed on a compositional reservoir model that incorporating geological, geophysical and engineering data, and this reservoir model has been successfully history matched with field data by calibrating it with 55 years primary and secondary production data and 8 years tertiary CO_2 – WAG data. The workflow is summarized in Figure 1.

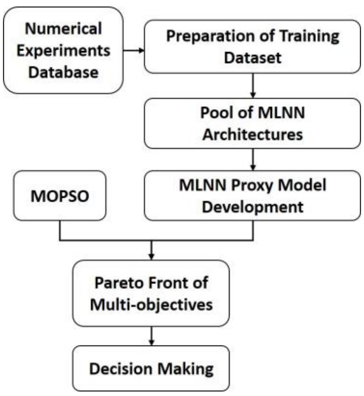

Figure 1 Procedures of optimization framework

Detailed procedures will be presented in following sections.

A. Data Preparation

Training data include complete inputs and outputs extracted from these 597 high-fidelity experiment runs. Training inputs are 4 parameters selected from a sensitivity analysis, including water cycle, gas cycle, producer bottomhole pressure (BHP) and water injection rate. Training targets are time series of cumulative oil production and CO_2 storage amount in next 20 years. 50 data points are extracted from each time series at equal time interval, which is to represent the entire time series.

For each numerical simulation run, two time series are extracted as training targets in this work: cumulative oil production and CO_2 storage, since the objectives need to be optimized are cumulative oil production at the end of 20 years forecasting time period and the amount of CO_2.

Figure 2 displays the structure of training dataset.

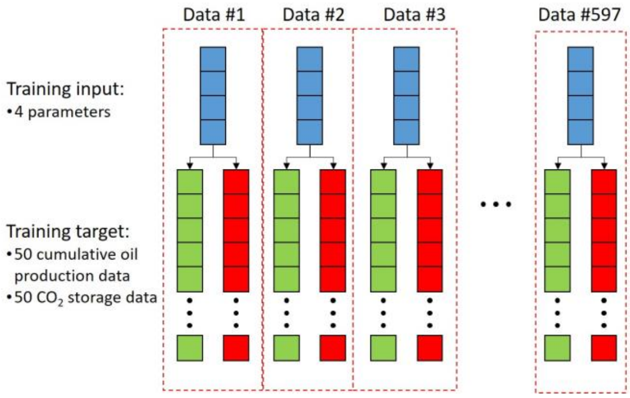

Figure 2 Structure of training dataset, the traing targets include cumulative oil production (green), CO_2 storage amount (red)

B. Development of Multi-layer Neural Network

A multi-layer neural network is composed of three types of layers: one input layer, one (or more) hidden layers and one output layer. The input information is transferred to hidden layers via weighted connections. The information is processed in neurons in hidden layers through the linear transformation function (activation function) and then transferred to the output layer. Connections between hidden layers and from hidden layer to output layer are controlled by weight vectors.

The architecture to be optimized in this work of a multi-layer feedforward neural network accounts for the number of neurons in each hidden layer, the number of hidden layers and activation functions used in each hidden layer. Since different architectures will influence the performance of the developed feedforward neural network, a pool containing different neural network architectures is generated in this work and the optimization framework will select the architecture that have best performance from this pool.

Considering the size of database used for this work, maximal number of hidden layer is set to be 5, and possible number of neurons in each hidden layer is preset to be selected from a close set [50, 200] due to the number of outputs constructed in training data. Possible options for the activation function used in this work include the hyperbolic tangent sigmoid transfer function (tansig) and the log-sigmoid transfer function (logsig). The framework will select the best architecture from the pool. For simplicity, a format is defined to represent possible combinations. For example, an architecture containing 3 hidden layers, with 60 neurons in the first layer, 70 neurons in the second layer and 80 neurons in the last layer will be expressed as {60, 70, 80} The number of values in the brace represents the number of hidden layer used in each architecture, and each value representing the number of neurons in each hidden layer. For example, {80} means only 1 hidden layer with 80 neurons is used.

For every training of network, the 597 training datasets will be randomly divided into three groups following the ratio of 80%, %10 and 10%. Among them, 477 sets of data will (80% of 597 runs) will be used to train the neural network. 60 sets of data (10% of 597 runs) will be used for validation purpose, while the other 60 sets of data are used in blind tests. The performance of the trained neural network is determined by finding the absolute relative error of blind test data that are not used in training the network. The absolute relative error of blind test data (E) in one training realization is calculated based on Eq. 1:

$$E = \frac{1}{m}\sum_{k=1}^{m}\frac{|T_k - Y_k|}{T_k} \quad (1)$$

where T_k is the observed target value of k-th output, Y_k is the predicted value of k-th output, m is the number of outputs of each experiment.

In this work, each of architecture picked from the architecture pool will be train 10 times repeatedly. For each training work, the training data, validation data and test data are randomly selected from the 597 data sets following aforementioned ratios, which is to make sure every training realization will use different training data. The alternation of test data in every training realization also guarantees the trained network can be tested in a broader range of data that are not used for training and validation purpose. Finally, the framework will find out the average absolute relative error of these 10 times training works (E_i), which is expressed by Eq. 2:

$$E_i = \frac{\sum_{s=1}^{10} E_s}{10} \quad (2)$$

where E_i is the average blind tests error of the i-th architecture; E_s is the blind tests error in s-th training.

III. Results

A. Optimal Architecture

Table I summarizes the specifications of the found optimal MLNN architectures.

Table I Summary of the Optimal MLNN Architecture Found

Number of hidden layer	5
Hidden layer neurons	{159,168,51,101,53}
Activation functions	{tansig, tansig, tansig, logsig, logsig}
Blind test error	0.54%

The average absolute error calculated in 10 training runs of this optimal architecture is 0.54%. Figure 3 displays the histogram of the absolute relative errors of 10 training runs. In each training run, 60 sets of numerical experiment data are used as blind tests data, thus a total of 600 sets of data are used to test the architecture in 10 training runs. As shown, 52.50% of the blind test data sets have an error less than 0.5%, 97.83% of them have an error less than 1%. There is only one data set found to have an absolute relative error lager than 2% (2.61%).

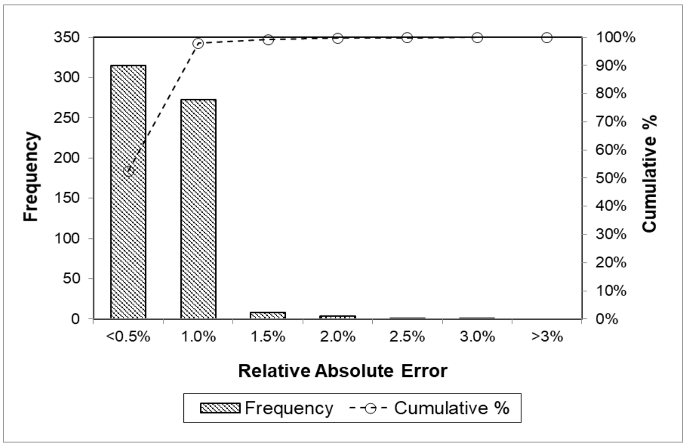

Figure 3 Histogram of blind tests results

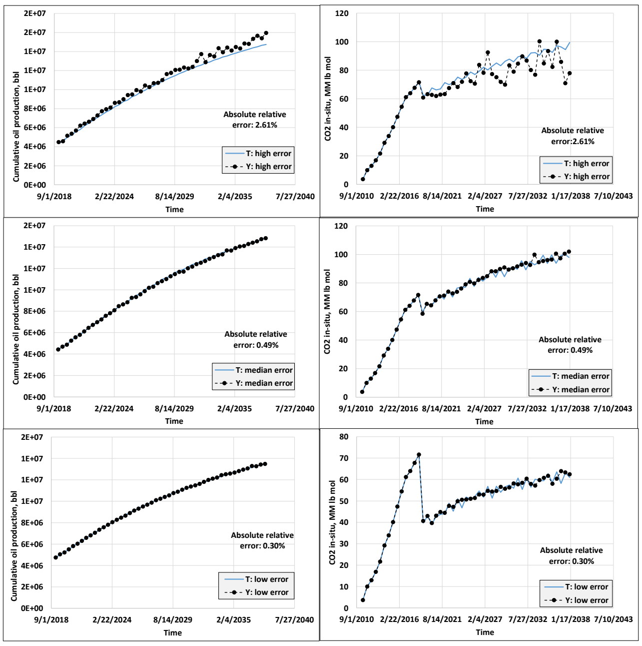

Figure 4 Comparison between Target Values and Predicted Values in 3 Selected Blind Tests

Figure 4 displays three data sets selected from all blind tests that yield to the lowest, median and the highest absolute relative error. The predictions made by trained proxy (Y) are compared with the observed simulation targets (T) in both CO_2 storage and cumulative oil production time series. A lower absolute relative error indicates a higher accuracy of predictions made by trained neural network proxy compared with observed simulation results. Among the 597 sets of blind test data, the worst one has a highest error of 2.61%, and this is the only one found to have an error lager than 2% (upper two plots in Figure 4). The median case (median two plots in Figure 4) and best case (lower two plots in Figure 4) have absolute relative error of 0.49% and 0.30% respectively. Although there exists some difference between proxy predictions and simulation targets, those cases with relatively higher errors only take a small part of all blind tests data. Figure 3 and Figure 4 strongly support that the proxy trained using optimal architecture is robust to make predictions matching well with observed simulation results from high-fidelity numerical model. The trained proxy can handle data with broad-range input parameters and make accurate predictions.

B. *Pareto Front*

The trained proxy using optimal architecture is utilized with MOPSO to generate the Pareto Front of two objectives considered in this work: predicted cumulative oil production (f_1, $\times 10^7$ barrels) and predicted CO_2 storage (f_2, $\times 10^6$ metric ton) at the end of next 20 years. The setup of MOPSO is listed in TABLE II.

TABLE II MOPSO Setup

Parameter	Value
Population size	300
Repository size	200
Inertia weight	0.4
Individual confidence factor	2.0
Swarm confidence factor	2.0
Uniform mutation percentage	0.5
Maximum number of generations	10,000 and 100,000

The repository size is set to be 200, which means the developed Pareto front will contain 200 nondominated solutions. The generated Pareto front of two objectives are displayed in Figure 5.

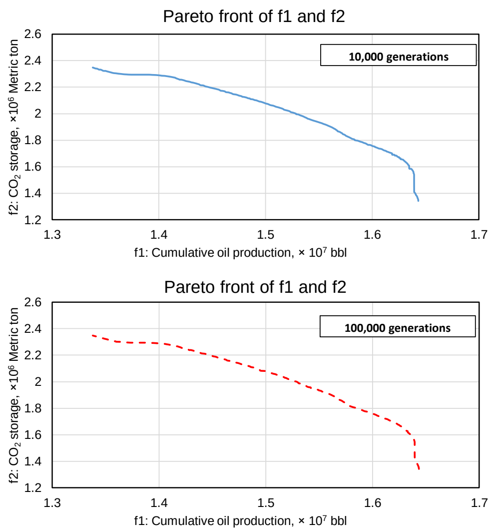

Figure 5 Pareto Front of Two Objectives Generated after 10,000 Generations and 100,000 Generations

A maximum of 10,000 generations was firstly set to generate the Pareto front, which is showed as the upper plot in Figure 5. Then, generations is augmented to 100,000 to generate the Pareto front once again to evaluate stability of developed Pareto front. It is found these two generated Pareto fronts are almost the same, indicating the stabilization of Pareto front. Figure 5 also indicates a range of f_1 and f_2 in generated Pareto front. As shown, range of f_1 of nondominated results is from 1.338 to 1.643, while range of f_2 is 1.343 to 2.347.

To validate the generated Pareto front, 5,000 experiments with different input parameters are conducted using the trained proxy. The parameters of these 5,000 experiments are randomly selected from their inputs range, as listed in TABLE III.

TABLE III Training Inputs

Parameters	Unit	Min	Max
Water injection period	day	100	200
Gas injection period	day	200	365
Producer BHP	psi	1000	4000
Water injection rate	stb/day	1000	3500

The results of these 5,000 random experiments are displayed in Figure 6. As shown, all solutions of these random experiments are dominated by the generated Pareto front.

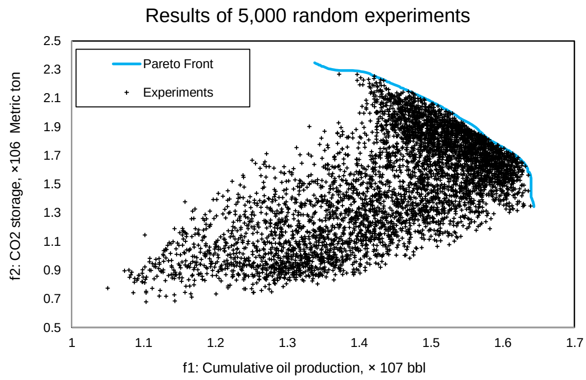

Figure 6 Comparison between Pareto Front and 5000 Random Experiments

The generated Pareto front is able to help make optimal decisions based on specific development desires. To use it efficiently, a trade-off factor τ between two objectives is defined as (3):

$$\tau = |\Delta f_2 / \Delta f_1| \tag{3}$$

where Δf_1 is the change in f_1, Δf_2 is the change in f_2. τ can indicate how much incremental CO_2 storage ($\times 10^{-1}$ metric ton) will be gained when oil production is reduced 1 barrel. And 1/τ is used to specify how much incremental oil production (barrel) will be obtained when CO_2 storage is decreased 1 $\times 10^{-1}$ metric ton. The value of trade-off factor indicates how much trade-off is needed to make when considering those two objectives: a larger τ indicates more oil production needs to be reduced when improving CO_2 storage, and a larger 1/τ indicates more CO_2 storage needs to be reduced when improving oil production. Pareto front is divided into 4 sections based on values of trade-off factor, which is showed in Figure 7.

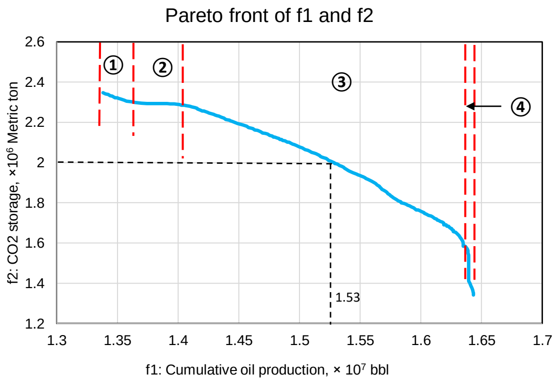

Figure 7 Sections Division of Pareto Front Based on Trade-off Factors

TABLE IV enumerates trade-off factors of these 4 sections.

TABLE IV Summary of Trade-off factors

Section	**1**	**2**	**3**	**4**
τ	0.5171	2.8937	0.3263	0.0200
$1/\tau$	1.9340	0.3456	3.0647	49.8824

Section 2 and section 4 have such a feature that improvement of one objective will cost relatively small reduction in the other objective. However, these two sections only occupy a small range of developed Pareto front, and major part is taken by section 1 and 3, which indicates when dealing with these two conflict objectives, trade-offs between them cannot be neglected.

Trade-off factor can be utilized to select target objective values based on different engineering desires. For example, if more oil production is emphasized in next 20 years production, then targets objective values should be selected from section 3 and 4, since values of f_1 of these sections are higher than other sections, which meaning a higher oil production. Comparing two sections, value of τ in section 3 is higher than that in section 4, which indicates a smaller trade-off needs to be made on CO_2 storage to obtain same amount of incremental oil production. Thus, the design objective values of f_1 and f_2 are recommended to be selected in section 3.

If the project needs more CO_2 to be stored in following 20 years, then target sections should be section 1 and section 2 where a higher CO_2 storage is observed. Section 1 has a higher value of $1/\tau$, indicating a smaller trade-off needs to be made on oil production to obtain the same amount of incremental CO_2 storage. Consequently, design objective values are recommended to be selected in section 1.

Another application of this Pareto front is choose optimal objective function value based on engineering or project requirements. For example, as of February 2019, 1.26×10^6 metric ton of purchased CO_2 had been stored within Morrow B sand. If the project requires an amount of 2×10^6 CO_2 metric ton storage in next 20 years, it is indicated by the Pareto front that the corresponding optimal cumulative oil production will be 1.53×10^7 barrels. The Pareto front can also tell the parameters used to achieve this optimal oil production.

C. *Comparison between Pareto Front and Weighted Sum Method*

When deal with problem with multiple objectives to optimize, Weighted Sum Method (WSM) combines different objectives into one aggregate function. Then, optimization algorithm is applied incorporated with aggregate equation to find the optimal solution. For comparison purpose, the aggregate equation (4) is also utilized in this work to find the optimal solution for these two objective functions.

$$f_t = f_1 + f_2 \tag{4}$$

where f_t is the combined objective function of f_1 and f_2, its unit is 10^6 metric ton CO_2 storage + 10^7 barrels oil.

Particle swarm optimization is applied coupled with f_t to find the best solution and it found an optimal solution with a value of 3.673. Then, the values of $f_1 + f_2$ of all solutions on Pareto front is calculated and plotted in Figure 8. It is found that the highest value of $f_1 + f_2$ in all Pareto front particles is 3.689, which is even higher than the solution found by using aggregate equation.

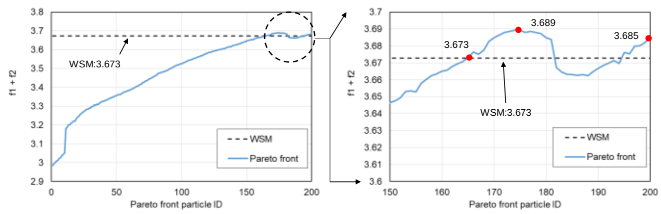

Figure 8 Comparison between Optimal Solution Found Using Aggregate Equation Coupled with PSO. The right Plot is Zoom in the Overlapped Part of the Left Plot

To furtherly investigate the difference between Pareto front and aggregate equation method, 3 solutions (cases) are picked from Pareto front to compare them with the unique optimal solution found using WSM. TABLE V lists f_t values of these four solutions.

TABLE V Comparasion between Unique Solutions Found Using WSM and Solutions Found Using Pareto Front

Case	**WSM**	**165**	**175**	**200**
$f_1 + f_2$	3.673	3.673	3.689	3.685

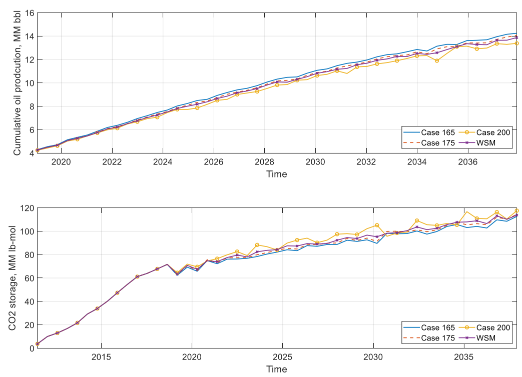

Figure 9 Cumulative Oil Production and CO_2 Storage Time Series of 4 Cases

It is found that Case 165 has the same f_t value with optimal solution found by PSO; Case 175 and Case 200 have even higher values. Optimal solutions found on Pareto front is the Case 175 with the value of 3.689. The cumulative oil production and CO_2 storage time series of these 4 cases are displayed in Figure 9.

There exists obvious difference between those 4 cases in their cumulative oil production and CO_2 storage time series. The comparison shows that:

1) Pareto front is capable to find a solution with a higher value of f_t than using WSM;

2) Pareto front will find all possible combinations of f_1 and f_2 to obtain the same value of f_t.

CONCLUSION

This work presents a robust machine-learning based computational framework that couples multi-layer neural network proxies and multi-objective particle swarm optimizer to design an active CO_2-WAG project undergoing at Farnsworth Unit. Significant conclusions obtained from this work involve:

(1) Developed Pareto front can indicate a range of non-dominated solutions of multi-objectives, and each of these solutions is with Pareto optimum so that one objective cannot be improved without impairing the other one. Since each solution is resulted from a combination of operational parameters, Pareto front will provide more options for project engineers to design a CO_2-WAG project.

(2) In this work, two trade-off factors are defined to use developed Pareto front more efficiently and hence assisting decision maker to make a decision on quick selection of objective values. Three applications cases of the trade-off factor are proposed as examples.

(3) For given criteria to determine optima, Pareto front proves the existence of non-unique solutions that result in the same optima. In this work, if the aggregate function f_t (Eq. 4) is used to determine optimal solution, it is observed that there exist different solutions with the same or very close value of f_t. Thus for those works employing WSM to transfer MOP to SOP, it is possibly found that various engineering designs can reach the same decision-making criteria, which gives engineers more flexibility to design a project to meet a certain objective function.

(4) In engineering practices, decision making could be restricted by various operational or engineering constraints. By using Pareto front, engineers can firstly choose all possible solutions that satisfy required objective functions, then filtering out those solutions meet with project design constraints. This scheme demonstrates to be an efficient and fast method to design a project with constraints to be considered.

The proposed optimization protocol brings new insights to optimization of MOPs in petroleum and energy industry. It would serve as a benchmark solution to MOPs for those fields or projects with conflict objectives to optimize.

ACKNOWLEDGEMENT

Funding for this project is provided by the U.S. Department of Energy's (DOE) National Energy Technology Laboratory (NETL) through the Southwest Regional Partnership on Carbon Sequestration (SWP) under Award No. DE-FC26-05NT42591.

REFERENCE

1. Faltinson, J.E. and B. Gunter, *Net CO2 stored in North American EOR projects.* Journal of Canadian Petroleum Technology, 2013. **50**(7): p. 55-60.
2. Han, Y., C. Park, and J.M. Kang. *Estimation of Future Production Performance Based on Multi-objective History Matching in a Waterflooding Project*. in *SPE EUROPEC/EAGE Annual Conference and Exhibition.* 2010. Society of Petroleum Engineers.
3. Tapia, J.F.D., et al., *Optimal CO2 allocation and scheduling in enhanced oil recovery (EOR) operations.* Applied energy, 2016. **184**: p. 337-345.
4. Enick, R. and D. Olsen, *Mobility and conformance control for carbon dioxide enhanced oil recovery (CO2-EOR) via thickeners, foams, and gels–a detailed literature review of 40 years of research.* Contract DE-FE0004003. Activity, 2012. **4003**(01).
5. Dai, Z., et al., *Uncertainty quantification for CO2 sequestration and enhanced oil recovery.* arXiv preprint arXiv:1411.4900, 2014.
6. Dai, Z., et al., *An integrated framework for optimizing CO2 sequestration and enhanced oil recovery.* Environmental Science & Technology Letters, 2013. **1**(1): p. 49-54.
7. Ampomah, W., et al., *Co‐optimization of CO2‐EOR and storage processes in mature oil reservoirs.* Greenhouse Gases: Science and Technology, 2017. **7**(1): p. 128-142.
8. Ampomah, W., et al., *Optimum design of CO 2 storage and oil recovery under geological uncertainty.* Applied Energy, 2017. **195**: p. 80-92.
9. Ampomah, W., et al., *Performance assessment of CO2-enhanced oil recovery and storage in the Morrow reservoir.* Geomechanics and Geophysics for Geo-Energy and Geo-Resources, 2017. **3**(3): p. 245-263.
10. White, M.D., et al., *Numerical simulation of carbon dioxide injection in the western section of the Farnsworth Unit.* Energy Procedia, 2014. **63**: p. 7891-7912.
11. Ampomah, W., et al. *An integrated approach for characterizing a sandstone reservoir in the Anadarko Basin.* in *Offshore Technology Conference*. 2016. Offshore Technology Conference.
12. Ampomah, W., et al. *Farnsworth field CO 2-EOR project: performance case history*. in *SPE improved oil recovery conference*. 2016. Society of Petroleum Engineers.
13. Ahmmed, B., et al., *Chemical effects of carbon dioxide sequestration in the Upper Morrow Sandstone in the Farnsworth, Texas, hydrocarbon unit.* Environmental Geosciences, 2016. **23**(2): p. 81-93.
14. Cui, Y., et al., *Multi-objective optimization methods and application in energy saving.* Energy, 2017. **125**: p. 681-704.